The Mineral Phase of Calcified Cartilage: Its Molecular Structure and Interface with the Organic Matrix

Melinda J. Duer,[†*] Tomislav Friščić,[†] Rachel C. Murray,[‡] David G. Reid,[†] and Erica R. Wise[†]
[†]Department of Chemistry, University of Cambridge, Cambridge, United Kingdom; and [‡]Animal Health Trust, Newmarket, United Kingdom

ABSTRACT We have studied the atomic level structure of mineralized articular cartilage with heteronuclear solid-state NMR, our aims being to identify the inorganic species present at the surfaces of the mineral crystals which may interact with the surrounding organic matrix and to determine which components of the organic matrix are most closely involved with the mineral crystals. One-dimensional ^{1}H and ^{31}P and two-dimensional ^{1}H-^{31}P heteronuclear correlation NMR experiments show that the mineral component is very similar to that in bone with regard to its surface structure. $^{13}C\{^{31}P\}$ rotational echo double resonance experiments identify the organic molecules at the mineral surface as glycosaminoglycans, which concurs with our recent finding in bone. There is also evidence of γ-carboxyglutamic acid residues interacting with the mineral. However, other matrix components appear more distant from the mineral compared with bone. This may be due to a larger hydration layer on the mineral crystal surfaces in calcified cartilage.

INTRODUCTION

Degenerative joint diseases such as osteoarthritis (OA) are a major problem in the developed world, where advances in medical care have resulted in a substantial elderly population who are at risk. The symptoms include chronic pain and loss of mobility, causing a significant decrease in quality of life for the sufferer, even when their pain can be controlled. Primarily considered to be an affliction of the cartilage, OA also results in changes to the underlying bone that thickens and sometimes misshapes, enhancing the effect of wear-and-tear on the joint degradation. What is not yet clear is the contribution of the zone of calcified cartilage (ZCC) to the progression of OA or the effect of OA on the ZCC. The ZCC is the deepest zone of articular cartilage which covers the ends of bones at the joint surfaces. Its structure and material properties have been far less extensively studied than those of bone; however, a good understanding of the structure and role of the ZCC in a healthy joint is crucial to elucidating its role in diseases such as OA.

In the long bones of a developing mammalian embryo, cartilage at the growth plate becomes calcified and is subsequently replaced by bone tissue. This process is known as endochondral ossification and results in lengthening of the bone (1). In the adult skeleton, only the layer of mineralized cartilage at the ends of long bones beneath articular cartilage remains, and this constitutes the ZCC. The rate at which endochondral ossification occurs in the ZCC to replace cartilage with bone is far slower than in the growth plate of an immature skeleton (2,3). The ZCC provides the contact between soft cartilage and the underlying bone, allowing transmission of forces, and affects the ability of nutrients to diffuse between the tissues (4). It is accepted that the total thickness of cartilage is greater at mature joint surfaces experiencing larger loads, but the relationship with the thickness of the ZCC is less clear (5–8). In osteoarthritic joints, the rate of endochondral ossification increases, resulting in loss of articular cartilage and hypermineralization of the ZCC, leading to increased stiffness (2). The thinning of the soft cartilage layer coupled with thickening of underlying bone and increased stiffness of the ZCC only serves to accelerate the rate of OA progression (9).

Studies of the structure and composition of mineralized cartilage tissue in a normal mature joint are important steps toward determining changes occurring from OA, and how to limit these changes. Much of the work so far has used microscopy techniques such as scanning electron microscopy (10,11), transmission electron microscopy (11), light microscopy (4,11,12), and three-dimensional reconstruction of micrographs (13), to study the ZCC, including obtaining data such as the location of its cells and blood vessels relative to structural features. These techniques have been used in conjunction with nanoindentation (2) and scanning small-angle x-ray scattering (12) to obtain information on material properties and mineral particle orientation, respectively. Quantitative backscattered electron imaging has been used to measure the microscopic variation in degree of mineralization across a sample. Studies have shown mineralization levels to be higher than in bone, although they are rather variable in different regions of calcified cartilage (3,12). Articular calcified cartilage from patients with OA was found to have some hypermineralized regions, with a corresponding hardness approximately twice that of bone (2). Although ultimately useful, these methods have the major disadvantage of requiring sample preparation which may alter the structure of the tissue, so other experiments are a necessary requirement

Submitted August 21, 2008, and accepted for publication December 15, 2008.

*Correspondence: mjd13@cam.ac.uk

Editor: Marc Baldus.

0006-3495/09/04/3372/7 $2.00

doi: 10.1016/j.bpj.2008.12.3954

to ensure that observations are not due to artifacts of sample preparation.

At a molecular level, vibrational spectroscopy methods (infrared (9,14,15) and Raman (14)) have been used to find relative proportions of protein, phosphate, and carbonate, as well as a comparison of crystallinity, crystal size, and collagen cross-linking in samples. Studies of mineralized cartilage by nuclear magnetic resonance (NMR) are confined to tissue from the growth plate rather than the joint surface. ^{31}P NMR spectra show the existence of HPO_4^{2-} in a non-crystalline environment in the mineral component of growth plate cartilage of calves (16). NMR microscopy has been used to identify different tissue zones across embryonic avian growth plate on the basis of their water proton transverse relaxation times (17).

Overall, the studies to date on the ZCC have shown that the mineral component is a substituted form of hydroxyapatite, quite probably similar to that in bone. Carbonate is present as a substitution in the mineral, as confirmed by Fourier transform infrared spectroscopy (16,18,19), but the concentration is found to differ from that in bone mineral (16,19). Similar size distributions for the mineral crystals are found for bone and mineralized cartilage (12,20), using x-ray diffraction. The underlying organic matrix of mineralized cartilage is mainly a mixture of types II and X collagen and glycosaminoglycans, such as chondroitin sulfate. The collagen forms bundles of triple helices, which provide a scaffold for the deposition of calcium phosphate mineral particles. The glycosaminoglycans are usually present as components of proteoglycans, where their long sugar chains are covalently attached to a protein core.

What is still lacking is a detailed study of how the mineral phase of the ZCC interacts with the organic matrix at a molecular level. This study seeks to address that with a combination of ^{31}P and ^{1}H NMR to determine the nature of inorganic species at the mineral crystal surfaces and ^{13}C-^{31}P double resonance NMR to examine which parts of the organic matrix are in close contact with those surfaces. The mineral crystals are expected to have surface structures and compositions significantly different from the bulk, as found in a recent comprehensive study of laboratory-prepared nanocrystalline hydroxyapatite (21). The nature of the crystal surfaces is clearly key in defining how the mineral is able to bind to the organic matrix, and therefore important to determine if we are to understand this binding. One-dimensional ^{1}H and ^{31}P and two-dimensional ^{1}H-^{31}P correlation NMR spectra in this work give invaluable insight into the nature of the surface species and their approximate concentrations.

We use the ^{13}C{^{31}P} rotational echo double resonance (REDOR) experiment to determine which parts of the organic matrix are in close proximity to the crystal surfaces. We have recently used this same methodology to study the mineral-matrix binding in bone (22) and established that it is glycosaminoglycans (GAGs) that are most closely bound in that tissue. Given the abundance of GAGs in mineralized cartilage, one of the driving forces behind this study is to see whether a similar binding mechanism operates in the ZCC. The REDOR experiment, as applied to ^{13}C and ^{31}P nuclei, allows the determination of which ^{13}C nuclei are close in space to ^{31}P nuclei (''close'' in this context being within ~6 Å). It utilizes the magnetic dipole coupling between ^{13}C and ^{31}P nuclei to dephase the signal from such ^{13}C, resulting in ^{13}C NMR spectra in which the signals from these nuclei are reduced in intensity. Thus, by comparing the REDOR spectra with reference spectra, we identify the ^{13}C functional groups most closely allied with ^{31}P nuclei, and because ^{31}P nuclei are largely confined to the mineral phase, by inference, the ^{13}C functional groups most closely allied with the mineral phase.

MATERIALS AND METHODS

Sample preparation

Tissue was harvested from horses used for general-purpose exercise, with no bone or joint abnormalities detected by clinical and histological examination, and euthanized for humane reasons unconnected with this study. Tissue without further preparation was stored at − 20°C when not undergoing manipulation or analysis. Articular mineralized cartilage (from the distal aspect of the proximal phalanx of an eight-year-old thoroughbred gelding, and from the distal radius of a 12-year-old mare) was removed from the underlying subchondral bone with a small band saw. The bone and mineralized cartilage samples were cut into small pieces, frozen in liquid nitrogen to retain components that are more volatile and maintain naturally occurring hydration levels, then powdered in a Dismembrator S ball mill (Sartorius Stedim Biotech, Springfield, MO). All samples were packed into 4 mm zirconia magic-angle spinning rotors. An adjacent sample from each site was retained for histological examination to confirm tissue homogeneity and absence of abnormalities. The γ-carboxyglutamate (free acid) was purchased from Sigma-Aldrich (St. Louis, MO).

XRPD measurements

X-ray powder diffraction experiments were performed on a Philips X'Pert Pro powder diffractometer equipped with an X'celerator RTMS detector, using Ni-filtered CuKα radiation (Philips Analytical, Amelo, The Netherlands). Data collection was performed in a 5–80° range using samples on a flat plate, with a scanning step size of 0.008°, time per step of 10.8 s, and scan speed of 0.0985°/s.

NMR experiments

^{31}P, ^{1}H, and ^{13}C experiments were carried out on an Avance 400 spectrometer operating at 162.1 MHz for ^{31}P, 400.4 MHz for ^{1}H, and 100.7 MHz for ^{13}C (Bruker BioSpin, Billerica, MA). All experiments were conducted at ambient temperature using standard Bruker 4 mm magic-angle spinning probes, including a broadband tunable triple resonance probe for the REDOR work. Magic angle spinning was used in all experiments to remove the line-broadening effects of nuclear spin interactions. The spinning rates used were 8.5 kHz for proton experiments and 12.5 kHz for heteronuclear correlation (HETCOR) and REDOR experiments. ^{1}H spectra were acquired using an excitation pulse of 2.6 μs and a recycle delay of 4 s. For the ^{1}H-^{31}P HETCOR experiments, a 2.6 μs $\pi/2$ pulse was used for ^{1}H excitation before the t_1 period. This was followed by Lee-Goldburg cross polarization (LGCP) to ^{31}P with a contact time of 2 ms using a field strength of 50 kHz. A recycle delay of 4 s and a t_1 increment of 80 μs was used.

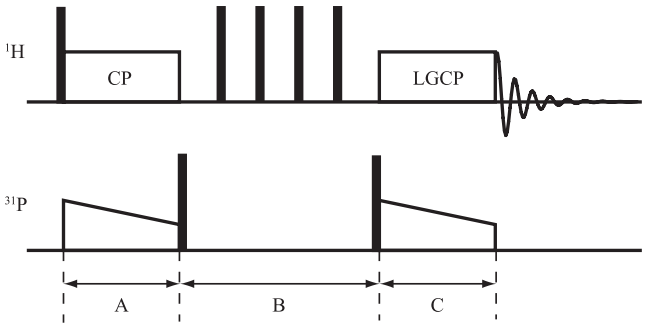

FIGURE 1 Pulse sequence used for spectral editing of ^{1}H spectra. During period *A*, magnetization is transferred from ^{1}H to nearby ^{31}P nuclei. In *B*, any remaining ^{1}H magnetization is suppressed by a series of saturation pulses before transferring ^{31}P magnetization back to ^{1}H during period *C*. Only signals due to ^{1}H close in space to ^{31}P are observed as CP is only efficient over short distances. LGCP is utilized in the CP step in period *C* to ensure the magnetization is not transferred to more distant protons via spin diffusion.

Spectra showing only the signals from protons close in space to ^{31}P were acquired using the pulse sequence shown in Fig. 1. These experiments used 2.6 μs $\pi/2$ pulses for ^{1}H excitation and the saturation period. The first CP step used a contact time of 2 ms. ^{31}P magnetization was stored along z for the duration of the proton saturation using a 2.8 μs pulse. The $\pi/2$ pulses were applied to ^{1}H repetitively every 2.5 ms for a total of 80 ms. This was verified in a separate experiment to be sufficient to dephase all remaining ^{1}H magnetization by subsequent acquisition of a ^{1}H spectrum. LGCP was then used to transfer magnetization back to ^{1}H with a field strength of 50 kHz applied for 2, 5, or 8 ms. A 4 s recycle delay was left between consecutive scans of the experiment.

^{13}C{^{31}P} REDOR experiments were performed after cross polarization from ^{1}H to ^{13}C with a 2.5 ms contact time. A train of rotor-synchronized ^{31}P π pulses of duration 8.6 μs (with the center of each pulse 80 μs from its neighbors) was then applied to recouple the ^{31}P-^{13}C magnetic dipolar interaction. At the middle of the ^{31}P pulse train, a ^{13}C π pulse of duration 10 μs was applied to refocus the ^{13}C magnetization. TPPM proton decoupling was applied during all heteronuclear signal acquisitions with a field strength of 96 kHz.

^{1}H spectra were referenced to the hydroxyl signal of hydroxyapatite (HAP) at 0.2 ppm relative to tetramethylsilane, ^{31}P spectra to the PO_4^{3-} signal of HAP at 2.6 ppm relative to H_3PO_4, and ^{13}C spectra to the methylene signal of glycine at 43.1 ppm relative to tetramethylsilane.

RESULTS AND DISCUSSION

The mineral component

Powder x-ray diffraction on both samples of mineralized articular cartilage produces diffraction patterns very similar to that of bone (Fig. 2), showing close correspondence to that given by hydroxyapatite (HAP, $Ca_{10}(PO_4)_6(OH)_2$). However, the reflections from the biological samples are broad, as found in previous work (1,23) indicating small crystals or disorder in the mineral component.

The ^{1}H NMR spectrum of mineralized cartilage is dominated by signals from the organic matrix. In principle, a ^{1}H spectrum of the mineral phase only may be obtained by cross polarizing from ^{31}P (primarily in the mineral) to ^{1}H, so-called reverse cross polarization (CP), as this restricts the ^{1}H signals to those from ^{1}H close in space to ^{31}P. Indeed, such methodology has been utilized in several cases for the study of bone (24,25), dental mineralized tissues (26), and synthetic calcium phosphates (27). Unfortunately, these experiments require long delays between scans because of the long T_1 values of ^{31}P within the mineral phase and hence long experiment times to achieve an adequate signal/noise ratio.

Here, we demonstrate that this inconvenience can be overcome by a prior CP period from ^{1}H to ^{31}P, as the required delay between scans is then governed by the T_1 of the mineral protons which is much shorter. The spectra in Fig. 3 *a* are obtained by CP from ^{1}H to ^{31}P, followed by a set of saturation pulses on ^{1}H to remove residual signal (see pulse sequence in Fig. 1), then LGCP back to ^{1}H. The resulting spectra for both samples of mineralized cartilage shows three broad proton signals between ~0 and 20 ppm, which are reminiscent of those found for bone (28), including their variation in intensity with contact time as shown in Fig. 3, and so may be assigned similarly. The narrowest of these signals, centered at 0.2 ppm, is assigned to the hydroxyl protons of a HAP-like phase (21). The signal at 5.2 ppm is assigned to H_2O in close proximity to ^{31}P,

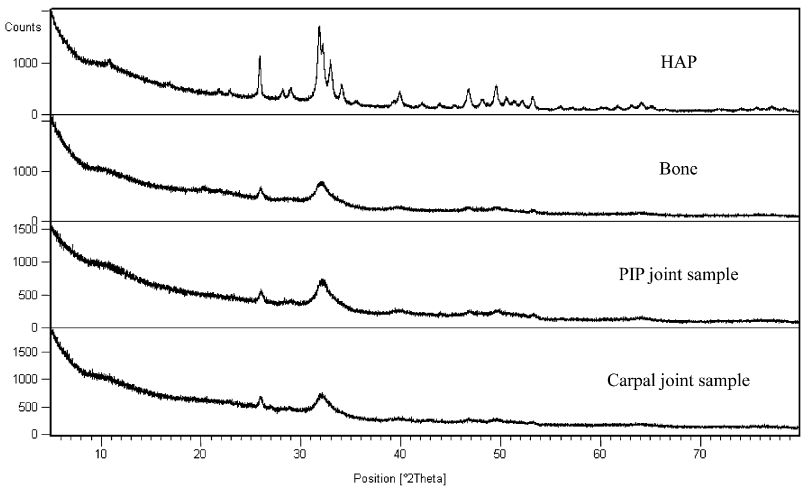

FIGURE 2 X-ray powder diffraction patterns of HAP, equine bone, and mineralized equine cartilage from the PIP joint and carpal joint.

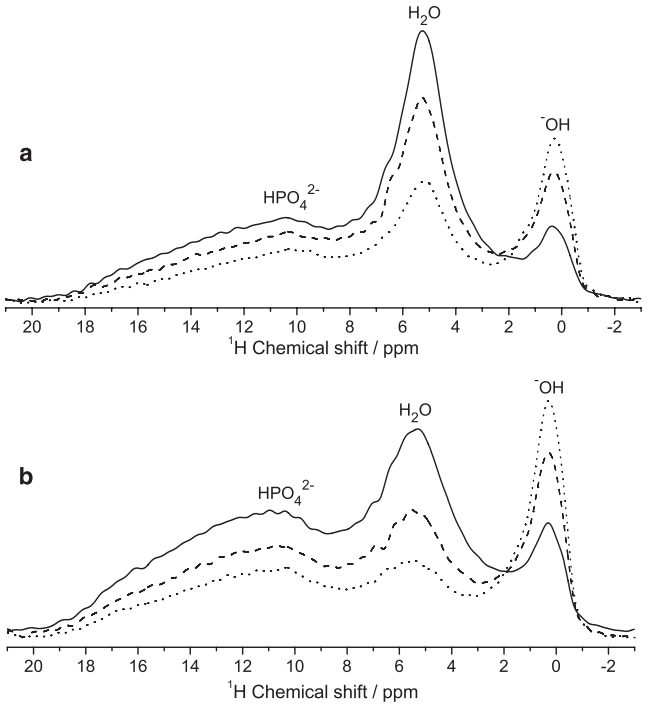

FIGURE 3 Spectra of the mineral protons of (*a*) PIP joint mineralized cartilage and (*b*) bone using the pulse sequence shown in Fig. 1. The second CP step, ^{31}P to ^{1}H (period *C* in the pulse sequence) used contact times of 2 ms (*solid line*), 5 ms (*dashed line*), and 8 ms (*dotted line*); all other experimental details were identical. The spinning rate was 8.5 kHz and 4096 scans were accumulated for each spectrum. Proton-containing species assigned to the signals are indicated.

either hydrogen-bonded to the mineral surface or included in the structure. The third signal is very broad and is assigned to HPO_4^{2-} on the basis of its chemical shift (centered at 10.2 ppm) (21,29).

The key point now is to identify which of these species, ^-OH, H_2O, and HPO_4^{2-}, are present on the surface of the mineral crystals in mineralized cartilage and therefore have the potential to interact with the organic matrix in this tissue. To examine this, we utilize ^{1}H-^{31}P HETCOR NMR spectra of the samples. Such a spectrum correlates ^{1}H signals with the ^{31}P spectra of those ^{31}P which are close in space to the particular ^{1}H nuclei. The correlation is produced experimentally by Lee-Goldburg cross polarization from ^{1}H to ^{31}P in the mixing period of the two-dimensional pulse sequence. The spectrum thus very largely contains signals from the mineral component only, as there is relatively little phosphorus in the organic matrix (28,30) and mineral ^{31}P nuclei are too far away from the organic matrix ^{1}H to allow significant CP between them. This feature has been used in previous work on bone (31,32,28). Furthermore, the linewidth of the ^{31}P signals allows us to assign them (21,29,32–34) (and through them, the correlated ^{1}H signals also) to surface or bulk regions of the mineral crystals, as the bulk is expected to be relatively well ordered and crystalline and hence give relatively sharp ^{31}P NMR lines, while the surface regions, because of their interactions with the organic matrix beyond, are expected to have somewhat more heterogeneous environments and hence broader ^{31}P lines.

A ^{1}H-^{31}P HETCOR spectrum of one of the mineralized cartilage samples is shown in Fig. 4. As expected, there are proton signals at 0.2 ppm from the mineral hydroxyl groups, 5.2 ppm from mineral-bound water and 10.2 ppm from HPO_4^{2-}, all correlated to ^{31}P. The hydroxyl signal at 0.2 ppm is correlated to a ^{31}P peak which is relatively sharp compared with the ^{31}P signals correlated with other ^{1}H signals in the spectrum, suggesting that the hydroxyl groups are in relatively well-ordered environments; it should be noted that this linewidth is still significantly broader than what one would expect for highly crystalline, macroscopic particles. The H_2O ^{1}H peak at 5.2 ppm is correlated to a much broader ^{31}P signal, suggesting it is dominated by the contribution of heterogeneous, surface-bound water. The ^{31}P signal correlated to 10.2 ppm in the proton dimension has a similar breadth to the H_2O-correlated signal and so is also assigned primarily to surface species. This makes sense, as surface ions are coordinatively unsaturated, so reducing their charge by protonation, i.e., phosphate to hydrogen phosphate, reduces the imbalance of electrostatic forces which otherwise occurs at the surface of the crystal. This is also consistent with previous findings on bone mineral (24).

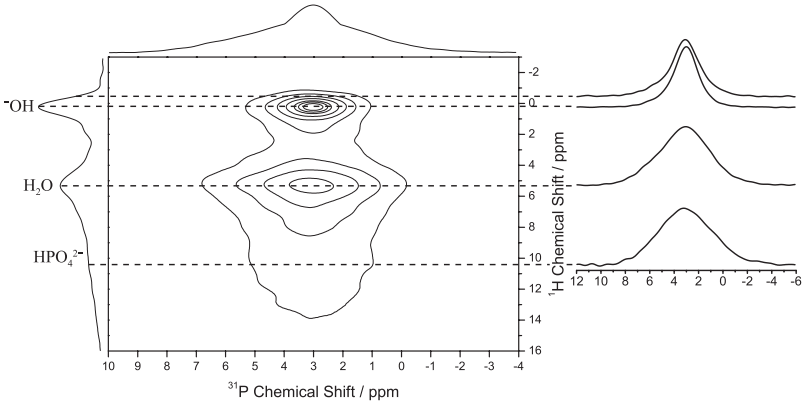

FIGURE 4 A typical two-dimensional ^{1}H-^{31}P HETCOR spectrum of PIP joint mineralized cartilage. A mixing time of 2 ms was used and 50 t_1 increments with 256 scans per increment. The traces on the right are cross sections through the spectrum at selected ^{1}H chemical shifts; effectively, they represent the characteristics of the mineral ^{31}P associated with ^-OH (− 0.5 and 0.2 ppm), H_2O (5.2 ppm), and HPO_4^{2-} (10.2 ppm) species.

The mineral-matrix interface

A ^{13}C NMR spectrum of one of the mineralized cartilage samples is shown in Fig. 5. The spectrum is very similar in form to that of bone, which is not surprising as both tissues contain collagen as their principal organic component. Most of the signals may be assigned to the common amino acids of collagen, as in spectra of bone and cartilage (30,35–40). However, several signals cannot be accounted for by protein, including the broad peaks at ~103 and 76 ppm. These have been assigned to GAGs in bone and mineralized cartilage (22) and some more detailed assignments are indicated in Fig. 5 with reference to chondroitin sulfate, an abundant GAG in cartilage, although it is likely that other GAGs (such as hyaluronic acid) also contribute to the signal.

$^{13}C\{^{31}P\}$ REDOR experiments have been carried out on both samples of mineralized cartilage to investigate the organic-mineral interface. Typical results are shown in Fig. 6, *a* and *b*, which also compares the mineralized cartilage results with those from a sample of adult equine subchondral bone in Fig. 6 *c*. A pair of spectra are shown for each sample: a reference spectrum and a REDOR spectrum in which signals from ^{13}C that are close in space to ^{31}P nuclei show a decrease in intensity as described in the Introduction. The closer the ^{13}C and ^{31}P nuclei are, the greater the decrease in the intensity of the ^{13}C signal, known as dephasing, in the REDOR spectrum.

As in bone (22), and other naturally mineralized tissues like dentine (41), the signals that show the greatest dephasing in mineralized cartilage are: a broad shoulder centered at ~181 ppm on the envelope of signals contributed mainly by protein carbonyl groups and mineral carbonate; a protein carbonyl (or in general, amide) signal at ~172 ppm; and a signal in the aliphatic region at ~76 ppm. These signals

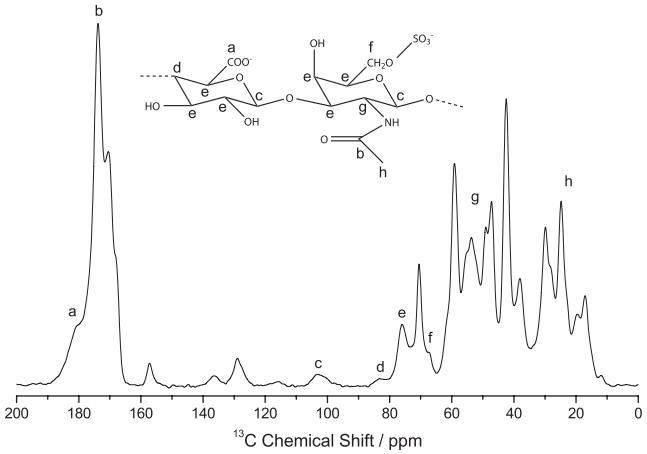

FIGURE 5 ^{13}C CP NMR spectrum of PIP joint mineralized cartilage acquired using a spinning rate of 12.5 kHz. An ^{1}H to ^{13}C CP contact time of 2.5 ms was used and 40,960 scans were accumulated. Some assignments to carbon atoms in glycosaminoglycans, typified by the common GAG chondroitin sulfate, are indicated. Several of the signals indicated also contain major contributions from protein functional groups.

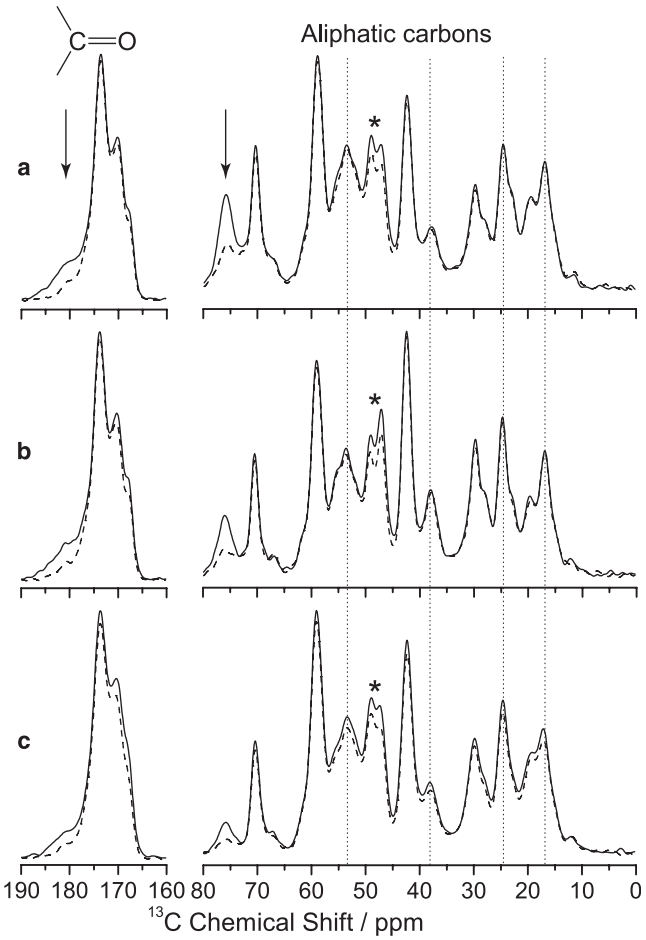

FIGURE 6 $^{13}C\{^{31}P\}$ REDOR spectra of mineralized cartilage from (*a*) the PIP joint, (*b*) the carpal joint, and (*c*) bone at a REDOR dephasing time of 8 ms. The reference spectra as described in the text are shown by solid lines and the REDOR spectra by dashed lines. Decreases in intensity between the solid and dashed lines show the effects of the ^{31}P-^{13}C interaction between the mineral ^{31}P and the organic matrix ^{13}C and hence identify those signals from nuclei in the latter which are close to the mineral surface. Vertical arrows indicate the signals, at ~76 ppm and 181 ppm, which dephase strongly in both materials. Dotted vertical lines emphasize those signals that dephase, not as strongly but consistently, in bone but to a much lesser extent or not at all in mineralized cartilage. Asterisks highlight other signals (at 47 and 49 ppm), that dephase consistently in both tissues, and may correspond to the γ-carboxyglutamate residues in Gla proteins.

are consistent, respectively, with carboxylate and amide groups, which could be in GAGs and/or proteins, and with some of the pyranose ring carbons of GAG polysaccharides. Additional signals in the range expected for other GAG ring carbons also show dephasing but it should be noted that these signals in the aliphatic region could be due to a variety of other components also. GAGs have been shown on many occasions to bind to bone mineral and have been invoked in both templating and inhibitory roles. Their anionic side chains (carboxylate and sulfate) are available to bind to calcium in the mineral crystal surfaces as well as their hydroxyl groups being involved in a multitude of

hydrogen-bonding interactions with surface water, mineral hydroxyl, and various phosphate ions.

In all adult equine bone samples we have examined, we also observe less prominent but consistent decreases in intensity of certain other signals, both in the carbonyl/carbonate and the aliphatic regions of the spectrum. This argues for some involvement of matrix proteins, including collagen, with the mineral surface in bone tissue, in addition to the major interaction with GAGs reflected by the strong dephasing of the 76 ppm signal. The dephasing of protein signals, however, is for the most part much less pronounced in both mineralized cartilage samples used in this work, exemplified by the signals connected by dotted vertical lines in Fig. 6. This argues that the connection between mineral and matrix proteins is less developed in mineralized cartilage than it is in bone, consistent with the more hydrated mineral surface we observe in the former tissue.

A striking exception to this is presented by the pair of signals at 47 and 49 ppm marked by asterisks in Fig. 6. There are of course many possible assignments of these signals, involving both amino acids and aminated ring carbons in GAGs. However, it is worth noting that γ-carboxyglutamic acid (Gla)-containing proteins are widely invoked as regulators of mineralization and that the γ-carbon of the Gla residue resonates at 49 ppm. The same residue almost certainly accounts for some of the signal at 181 ppm. This signal shows a REDOR effect, which may then be in part due to mineral proximity to the dicarboxylate groups in mineral-bound Gla-containing proteins. Thus, it is possible that REDOR is detecting the intimate involvement not only of GAGs, but of Gla-containing proteins at the mineral-organic interface.

The authors thank the UK Engineering and Physical Sciences Research Council (to E.R.W.) and Biotechnology and Biological Sciences Research Council (project No. BB/D013526/1, to D.G.R.) for funding.

REFERENCES

1. Glimcher, M. J. 2006. Bone: nature of the calcium phosphate crystals and cellular, structural, and physical chemical mechanisms in their formation. *Rev. Mineral. Geochem.* 64:223–282.
2. Ferguson, V. L., A. J. Bushby, and A. Boyde. 2003. Nanomechanical properties and mineral concentration in articular calcified cartilage and subchondral bone. *J. Anat.* 203:191–202.
3. Bullough, P. G., and A. Jagannath. 2004. Articular calcified cartilage canals in the third metacarpal bone of 2-year-old thoroughbred racehorses. *J. Anat.* 205:491–500.
4. Oegema, Jr., T. R., R. J. Carpenter, F. Hofmeister, and R. C. Thompson, Jr. 1997. The interaction of the zone of calcified cartilage and subchondral bone in osteoarthritis. *Microsc. Res. Tech.* 37:324–332.
5. Stougard, J. 1974. Calcified cartilage and subchondral bone under normal and abnormal conditions. *Acta Path. Micro. Im. A.* 82:182–188.
6. Lane, L. B., and P. G. Bullough. 1980. Age-related changes in the thickness of the calcified zone and the number of tidemarks in adult human articular cartilage. *J. Bone Joint Surg.* 62B:372–375.
7. Müller-Gerbl, M., E. Schulte, and R. Putz. 1987. The thickness of the calcified layer of articular cartilage: a function of the load supported? *J. Anat.* 154:103–111.
8. Muehleman, C., and K. E. Kuettner. 2000. Distribution of cartilage thickness on the head of the human first metatarsal bone. *J. Anat.* 197:687–691.
9. Miller, L. M., J. T. Novatt, D. Hamerman, and C. S. Carlson. 2004. Alterations in mineral composition observed in osteoarthritic joints of Cynomolgus monkeys. *Bone.* 35:498–506.
10. Duncan, H., J. Jundt, J. M. Riddle, W. Pitchford, and T. Christopherson. 1987. The tibial subchondral plate. A scanning electron microscopic study. *J. Bone Joint Surg. Am.* 69:1212–1220.
11. Boyde, A., and E. C. Firth. 1983. The morphology of the calcification front in articular cartilage. *J. Bone Joint Surg.* 65B:72–78.
12. Zizak, I., P. Roschger, O. Paris, B. M. Misof, A. Berzlanovich, et al. 2003. Characteristics of mineral particles in the human bone/cartilage interface. *J. Struct. Biol.* 141:208–217.
13. Lyons, T. J., S. F. McClure, R. W. Stoddart, and J. McClure. 2006. The normal human chondro-osseous junctional region: evidence for contact of uncalcified cartilage with subchondral bone and marrow spaces. *BMC Musculoskelet. Disord.* 7:52–59.
14. Boskey, A. L., and R. Mendelsohn. 2005. Infrared spectroscopic characterization of mineralized tissues. *Vib. Spectrosc.* 38:107–114.
15. Paschalis, E. P., O. Jacenko, B. Olsen, R. Mendelsohn, and A. L. Boskey. 1996. Fourier transform infrared microspectroscopic analysis identifies alterations in mineral properties in bones from mice transgenic for type X collagen. *Bone.* 19:151–156.
16. Rey, C., K. Beshah, R. G. Griffin, and M. J. Glimcher. 1991. Structural studies of the mineral phase of calcifying cartilage. *J. Bone Miner. Res.* 6:515–525.
17. Potter, K., W. J. Landis, and R. G. S. Spencer. 2001. Histomorphometry of the embryonic avian growth plate by proton nuclear magnetic resonance microscopy. *J. Bone Miner. Res.* 16:1092–1100.
18. Boskey, A. L., M. Maresca, B. Wikstrom, and A. Hjerpe. 1991. Hydroxyapatite formation in the presence of proteoglycans of reduced sulfate content—studies in the brachymorphic mouse. *Calcif. Tissue Int.* 49:389–393.
19. Kim, H. M., C. Rey, and M. J. Glimcher. 1996. X-ray diffraction, electron microscopy, and Fourier transform infrared spectroscopy of apatite crystals isolated from chicken and bovine calcified cartilage. *Calcif. Tissue Int.* 59:58–63.
20. Arsenault, A. L., and M. D. Grynpas. 1988. Crystals in calcified epiphyseal cartilage and cortical bone of the rat. *Calcif. Tissue Int.* 43:219–225.
21. Jaeger, C., T. Welzel, W. Meyer-Zeika, and M. Epple. 2006. A solid-state NMR investigation of the structure of nanocrystalline hydroxyapatite. *Magn. Reson. Chem.* 44:573–580.
22. Wise, E. R., S. Maltsev, M. E. Davies, M. J. Duer, C. Jaeger, et al. 2007. The organic-mineral interface in bone is predominantly polysaccharide. *Chem. Mater.* 19:5055–5057.
23. Vallet-Regi, M., and J. M. Gonzalez-Calbet. 2004. Calcium phosphates as substitution of bone tissues. *Prog. Solid State Chem.* 32:1–31.
24. Wu, Y., J. L. Ackerman, L. Graham, and M. J. Glimcher. 2005. Hydroxyl ions in bone mineral observed by 1D ^{31}P-^{1}H NMR spectroscopy. *J. Bone Miner. Res.* 20:S202–S203.
25. Kaflak, A., and W. Kolodziejski. 2008. Kinetics of ^{1}H $\rightarrow$ ^{31}P NMR cross-polarization in bone apatite and its mineral standards. *Magn. Reson. Chem.* 46:335–341.
26. Kolmas, J., and W. Kolodziejski. 2007. Concentration of hydroxyl groups in dental apatites: a solid-state ^{1}H MAS NMR study using inverse ^{31}P to ^{1}H cross-polarization. *Chem. Commun.* 42:4390–4392.
27. Crosby, R. C., R. L. Reese, and J. F. Haw. 1988. Cross polarization magic angle spinning proton NMR spectroscopy of solids. *J. Am. Chem. Soc.* 110:8550–8551.
28. Cho, G., Y. Wu, and J. L. Ackerman. 2003. Detection of hydroxyl ions in bone mineral by solid-state NMR spectroscopy. *Science.* 300:1123–1127.
29. Maltsev, S., M. J. Duer, R. C. Murray, and C. Jaeger. 2007. A solid-state NMR comparison of the mineral structure in bone from diseased joints in the horse. *J. Mater. Sci.* 42:8804–8810.

30. Schulz, J., M. Pretzsch, I. Khalaf, A. Deiwick, H. A. Scheidt, et al. 2007. Quantitative monitoring of extracellular matrix production in bone implants by ^{13}C and ^{31}P solid-state nuclear magnetic resonance spectroscopy. *Calcif. Tissue Int.* 80:275–285.

31. Santos, R. A., R. A. Wind, and C. E. Bronnimann. 1994. ^{1}H CRAMPS and ^{1}H-^{31}P HetCor experiments on bone, bone mineral, and model calcium phosphate phases. *J. Magn. Reson. B.* 105:183–187.

32. Wilson, E. E., A. Awonusi, M. D. Morris, D. H. Kohn, M. M. J. Tecklenburg, et al. 2006. Three structural roles for water in bone observed by solid-state NMR. *Biophys. J.* 90:3722–3731.

33. Tseng, Y.-H., Y.-L. Tsai, T. W. T. Tsai, J. C. H. Chao, C.-P. Lin, et al. 2007. Characterization of the phosphate units in rat dentin by solid-state NMR spectroscopy. *Chem. Mater.* 19:6088–6094.

34. Tseng, Y.-H., Y. Mou, P.-H. Chen, T. W. T. Tsai, C.-I. Hsieh, et al. 2008. Solid-state P-31 NMR study of the formation of hydroxyapatite in the presence of glutaric acid. *Magn. Reson. Chem.* 46:330–334.

35. Aliev, A. E. 2005. Solid-state NMR studies of collagen-based parchments and gelatin. *Biopolymers.* 77:230–245.

36. Huster, D., L. Naji, J. Schiller, and K. Arnold. 2004. Dynamics of the biopolymers in articular cartilage studied by magic angle spinning NMR. *Appl. Magn. Reson.* 27:471–487.

37. Huster, D., J. Schiller, and K. Arnold. 2002. Comparison of collagen dynamics in articular cartilage and isolated fibrils by solid-state NMR spectroscopy. *Magn. Reson. Med.* 48:624–632.

38. Reichert, D., O. Pascui, E. R. deAzevedo, T. J. Bonagamba, K. Arnold, et al. 2004. A solid-state NMR study of the fast and slow dynamics of collagen fibrils at varying hydration levels. *Magn. Reson. Chem.* 42:276–284.

39. Saitô, H., and M. Yokoi. 1992. A ^{13}C NMR study on collagens in the solid state: hydration/dehydration-induced conformational change of collagen and detection of internal motions. *J. Biochem.* 111:376–382.

40. Zernia, G., and D. Huster. 2006. Collagen dynamics in articular cartilage under osmotic pressure. *NMR Biomed.* 19:1010–1019.

41. Reid, D. G., M. J. Duer, R. C. Murray, and E. R. Wise. 2008. The organic-mineral interface in teeth is like that in bone and dominated by polysaccharides: universal mediators of normal calcium phosphate biomineralization in vertebrates? *Chem. Mater.* 20:3549–3550.